Multi-messenger science with Athena and Future Multi-messenger Observatories

Luigi Piro

INAF – Istituto di Astrofisica e Planetologia Spaziali, via Fosso del Cavaliere 100, I-00133
Rome, Italy
email: luigi.piro@inaf.it

Abstract. Scientific synergies between Athena and some of the key multi-messenger facilities that should be operative concurrently with Athena are presented. These facilities include LIGO A+, Advanced Virgo+ and future detectors for ground-based observation of gravitational waves (GW), LISA for space-based observations of GW, IceCube and KM3NeT for neutrino observations, CTA for very high energy observations. Multimessenger synergy science themes discussed here include pressing issues in the field of Astrophysics, Cosmology and Fundamental physics such as: the central engine and jet physics in compact binary mergers, accretion processes and jet physics in SMBBHs and in compact stellar binaries, the equation of state in neutron stars, cosmic accelerators and the origin of cosmic rays, the origin of intermediate and high-Z elements in the Universe, the Cosmic distance scale and tests of General Relativity and Standard Model. Observational strategies for implementing the identified science topics are also discussed.

Keywords. gravitational waves, gamma rays: bursts, methods: data analysis, stars: neutron.

1. Introduction

Recent years witnessed a blossoming of multi-messenger astrophysics, in which gravitational waves (GWs), neutrinos, and photons provide complementary views of the universe. The astounding results obtained from the joint electromagnetic-gravitational wave observations of the compact binary merger GW170817 or from the neutrino-electromagnetic (EM) observations of the blazar TXS 056+056 showed the tremendous discovery potential of this field, that will be progressively exploited throughout the next decade, as observing facilities are deployed. A substantial step forward could be expected by early 2030s, when the second and third generations of GW and neutrino detectors will become operational.

A full exploitation of the potential of multi-messenger astronomy demands also capabilities in the X-ray band that are beyond those achievable by current and near future missions, but consistent with the performance planned for *Athena*. For example, population studies of X-ray counterparts to GW mergers at the distances probed by next generation of GW detectors require an X-ray sensitivity that only *Athena* can provide. In this paper we focus on some selected topics focussed on the synergies of Athena on GW's, VHE and neutrinos. The reader is referred to Piro *et al.* (2021) for a more detailed and comprehensive discussion.

2. *Athena* as a multi-messenger observatory

Athena†, Advanced Telescope for High ENergy Astrophysics, is the X-ray observatory large mission selected by the European Space Agency (ESA), within its Cosmic Vision

† www.the-athena-x-ray-observatory.eu

2015–2025 programme, to address the Hot and Energetic Universe scientific theme, and it is provisionally due for launch in the early 2030s. *Athena* will have three key elements to its scientific payload: an X-ray telescope with a focal length of 12 m and two instruments: a Wide Field Imager (WFI)‡ [Meidinger *et al.* (2020)] for high count rate, moderate resolution spectroscopy over a large Field of View (FoV) and an X-ray Integral Field Unit (XIFU)¶ [Barret *et al.* (2021)] for high-spectral resolution imaging.

Most of the sources targeted by multi-messenger astronomy are related to energetic phenomena, such as stellar explosions, compact objects (black hole [BH]; neutron star [NS]; white dwarf [WD]), accelerations sites at all scales, and transients. These are the main constituents of the *Athena* science themes and, as such, have driven the science performance of the mission, that are therefore already largely tuned for a multi-messenger approach. In this regard *Athena* provides a unique combination of performances for the benefit of multi-messenger astronomy.

• The large FoV (0.4 deg^2) catered by the WFI, boosted by the capability of carrying out mosaic or raster scans up to 10 deg^2, allows us to cover error boxes of GW, neutrino and VHE sources down to the unprecedented sensitivity enabled by *Athena* (next bullet). This capability, coupled with the much smaller number of serendipitous sources expected in X-rays than at lower frequencies, will help in discovering the EM counterpart.

• A sensitivity of 2×10^{-17}erg cm^{-2} s^{-1} enables the discovery and the characterization of the temporal evolution of the faintest X-ray counterparts of multi-messenger events, such as the X-ray kilonovae.

• The combination of large area and low background allows *Athena* to characterize the spectral properties of faint X-ray sources, important e.g. for constraining leptonic vs hadronic models in neutrino and VHE sources, or tracking the spectral evolution of afterglows of GRBs and GW mergers.

• A source positional accuracy of ≈ 1 arcsec allows a precise location of the counterpart, enabling follow-up observations by other large EM facilities with a narrow FoV.

• The high spectral resolution (2.5 eV) and imaging capabilities of the X-IFU enable searches of extremely faint narrow lines from a rich variety of sources, from WHIM to radioactive decay from kilonova remnants, as well as to uniquely characterize the sites of particle acceleration in the Universe.

• The reaction time to Target of Opportunity (ToO) (4 h) coupled with the large fraction of the sky accessible at any time (>50%) and the large effective area allow *Athena* to follow-up GRBs and other multi-messenger transients fast enough to a) gather an adequate number of photons to enable high resolution absorption spectroscopy with the X-IFU (Fig. 1); b) to detect dim and fastly decaying sources of counterparts of multi-messenger events.

3. *Athena* and ground-based GW observatories

Athena will observe the location of a binary neutron star (BNS), or a NS- black hole (BH) binary pinpointed by a combination of GW facilities like LIGO A+, Advanced Virgo+ and next generation interferometers, GRB prompt emission or kilonova observations.

The *Athena* mission's broad aim of understanding the hot and energetic universe has a number of themes that overlap with the ground-based GW detectors broad aims of understanding the gravitational universe. For example, both types of facilities have as goals to investigate the physics and astrophysics of compact objects in a general sense. This includes more specific areas such as (i) improving our understanding of the EoS in neutron stars, (ii) measuring the spins of BHs, (iii) looking for BHs at high redshifts,

‡ www.mpe.mpg.de/ATHENA-WFI
¶ x-ifu.irap.omp.eu/
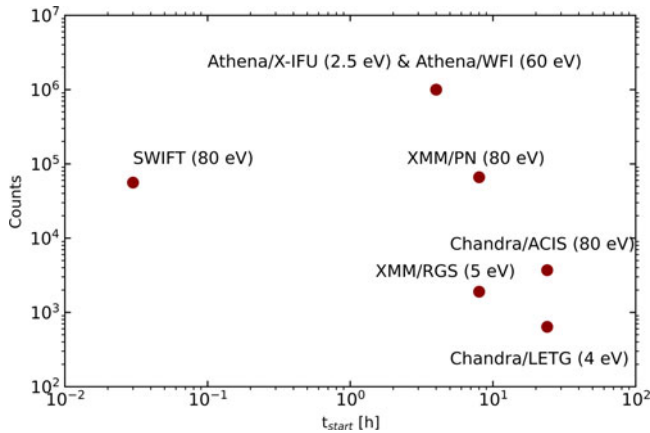
Figure 1. *Athena* capability on Targets of Opportunity (ToO). Number of counts gathered for a bright GRB integrated for about 50 ks as a function of the typical ToO response time for various instruments (energy resolution at 1 keV in parenthesis). The one million counts observed by *Athena* enable high resolution absorption spectroscopy of extremely weak lines.

(iv) determining the production sites of heavy elements, (v) improving our understanding of the engines powering SGRBs and the physics of jets, and (vi) learning about the environments around compact object mergers. Some of these themes can be done independently by *Athena* and GW detectors, and their results can provide useful complementary information. However, all of the themes are enhanced by having multi-messenger observations of the relevant events.

Future capabilities to observe and localize compact binary mergers are highlighted in Fig. 2 and Table 1. The left panel of Fig. 2 shows the detection horizons (solid lines) for four different detectors as a function of the total mass of the binary, for equal-mass non-spinning binaries. The detection horizon is the maximum distance that an optimally oriented binary can be detected. The distance here is represented as a redshift which was computed using a Λ-CDM model of cosmology [Ade *et al.* (2016)]. Also shown as shaded region is the 10% and 50% response distance, respectively. The response distance is a measure of detector sensitivity defined as the luminosity distance at which 10% (respectively 50%) of the sources would be detected, for sources placed isotropically on the sky with random orientations, and with all sources placed at exactly this distance. The right panel of Fig. 2 illustrates the number of two types of GW sources as a function of redshift: binary NSs with equal mass of 1.4 M$_\odot$ in yellow, and binary BHs with equal mass of 30 M$_\odot$ in white. The dotted-dashed lines are the horizons of the different ground-based detectors. The binaries are distributed to follow the Madau-Dickinson star-formation rate with a characteristic time delay of 100 Myr (see Vitale *et al.* (2019) for more details). Figure 3.1 shows that the next generation of GW detectors will have a significantly larger reach and thereby detect a much larger number of compact object mergers. In Table 1, we give numbers of expected NS-NS detections per year, localization areas, and number of detections with less than 1, 10, or 100 deg^2 localization areas for four possible detector networks [Sathyaprakash *et al.* (2019)]. The binaries were distributed in the same way as for the binary NSs shown in Fig. 2 with a local merger rate of 320 Gpc$^{-3}yr^{-1}$, which is consistent with the median rate inferred from LIGO's first three observing runs [Abbott *et al.* (2021)]. The number of detections per year varies by many orders of magnitude depending upon the specific detector configuration. In the most conservative scenario, there will be tens of NS-NS events localized to better than 10 deg^2 per year; in the most optimistic scenario, this becomes of order 104 events with
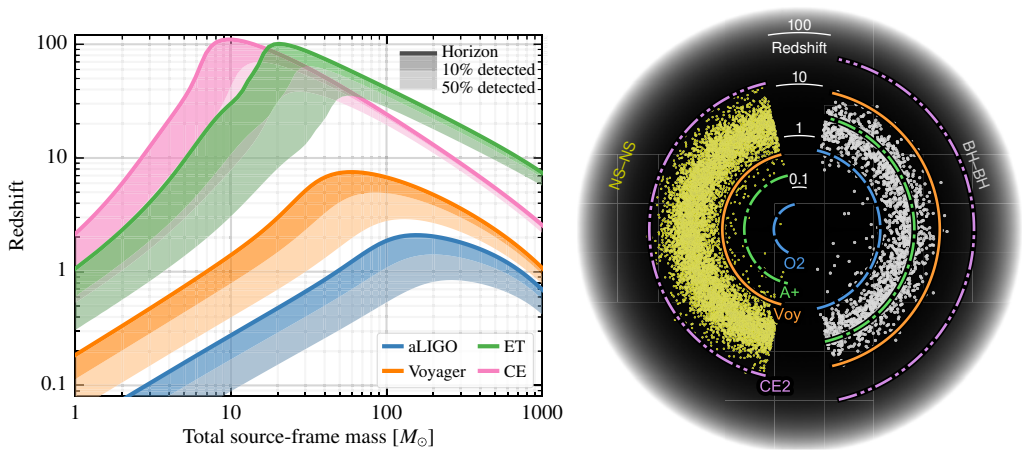
Figure 2. *Left*: Detection horizons and 10% and 50% response distances for four GW detectors, LIGO A+ (aLIGO in the figure), LIGO Voyager, ET, and CE, as a function of the binary's mass, for equal-mass binaries. Figure available from Hall (2019a) and appears in Hall *et al.* (2019b). *Right*: Populations of binary NSs (left half) and binary BHs (right half) for binaries that follow the Madau-Dickinson star-formation rate with a characteristic delay time of 100Myr. Also shown are the detection horizons of different GW detectors. The figure is available from Hall *et al.* (2019c).

Table 1. NS-NS Detections per year, localization, and localization rate estimates for different detector configurations. Numbers were computing assuming a Madau-Dickinson star formation rate, with a characteristic delay time of 100 Myr as in Vitale *et al.* (2019). A local co-moving NS-NS merger rate of 320 Gpc^{-3} yr^{-1} was assumed.

| Network	N(detected) [yr^{-1}]	Median loc. [deg^2]	N(<1 deg^2) [yr^{-1}]	N(< 10 deg^2) [yr^{-1}]	N(< 100 deg^2) [yr^{-1}]
HLVKI	15	7	0	15	15
3Voyager	800	20	5	170	770
1ET+2Voyager	6,100	21	20	960	6,100
1ET+2CE	320,000	12	4,500	130,000	310,000

a localization of less than one deg^2 per year. Given the number of well-localized mergers, one can expect that EM counterparts will be associated with a subset of them. NS-BH binaries are also a promising multi-messenger source for ground-based GW detectors and Athena.

Thanks to its superior sensitivity, *Athena* will play a key role in GRB and GW afterglow studies. With a detection threshold of 3×10^{-17} erg cm^{-2} s^{-1} in the 0.5-2.0 keV band (100 ks integration), *Athena* outperforms current X-ray facilities, such as the *Swift* X-ray Telescope and the *Chandra* X-ray Observatory, as well as future X-ray observatories in the search for orphan afterglows (i.e. those without a GRB counterpart) and off-axis afterglows (i.e. those seen at an angle from their jet-axis). This is illustrated in Fig. 3, showing the *Athena* sensitivity compared with an event similar to GRB 170817 at a range of orientations and distances.

Fig. 3 (left) shows characteristic X-ray light curves for a GW170817-like event, demonstrating the diversity of observable off-axis afterglow light curves. We briefly discuss a few specific goals for off-axis afterglow monitoring with *Athena* below:

• **Determine the rate of choked jets**. The afterglow light curve can be used to distinguish between successful and choked jets, as shown by Troja *et al.* (2018), and represents an important means by which *Athena* can help determine the outflow geometry (isotropic versus collimated) and eventually unveil a new population of X-ray transients
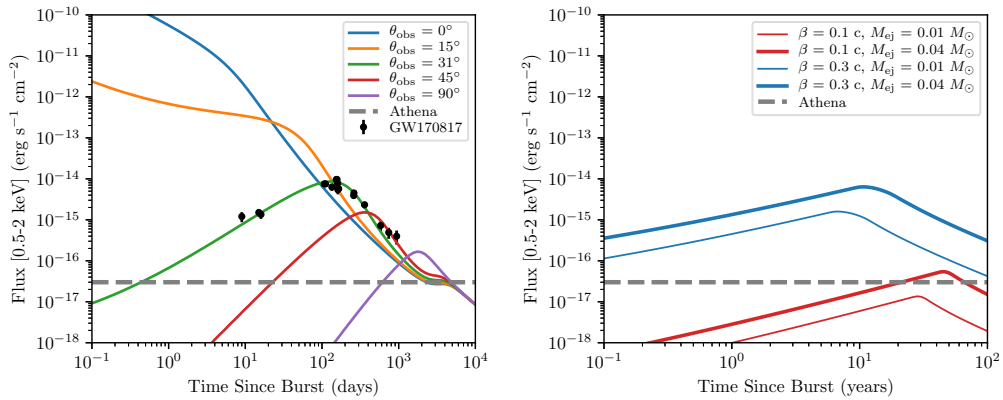
Figure 3. Left: light curves of a Gaussian 170817A-like jet at a distance of 41 Mpc at various viewing angles, parameters and X-ray data taken from Troja *et al.* (2020). Right: light curves of a kilonova afterglow at the same distance at different characteristic ejecta velocities and ejecta masses. The kilonova material has velocity stratification $k = 5$, the ambient medium is taken to have density $n_0 = 10^{-2}$ cm^{-3}, fiducial synchrotron parameters $p = 2.2$, $\epsilon_e = 10^{-1}$, and $\epsilon_B = 10^{-3}$. Both: fiducial *Athena* sensitivity of 3×10^{-17} erg s^{-1} cm^{-2} in 0.5-2 keV band.

produced by choked jets. Following the X-ray peak time, a slope steeper than 2, similar to the slope following the jet-break of a standard GRB, is characteristic of a collimated flow. GRB 170817 has indeed been confirmed to involve a successful jet by measurement of the late-time temporal slope of the afterglow light curve [Mooley *et al.* (2018); Troja *et al.* (2019); Lamb *et al.* (2019)]. Key observations using very-large baseline interferometry (VLBI, Ghirlanda *et al.* (2019); Mooley *et al.* (2018)), further established the jet nature.

● **Constrain jet geometry and orientation**. Normally, GRB afterglows are observed close to on-axis, with the bright prompt gamma-ray emission and early observations of a monotonically decaying afterglow providing a bottleneck for detection (see e.g. Nousek *et al.* (2006); Zhang *et al.* (2006)). GW observations are instead less biased towards on-axis events, and herald bursts whose collimated outflows are likely oriented at an angle relative to the observer. Depending on the lateral energy distribution of the jet, the observer angle and the jet opening angle, the afterglow light curve can be expected to show a rising stage first (as was the case for GRB 170817A). The early stage of the jet can also include signatures that constrains the physics of the ejecta, in particular its magnetization and Lorentz factor. Within the context of the off-axis light curves shown in Fig. 3, the implication is that for an event seen at angles up to $\sim 20°$, *Athena* will be uniquely capable of probing the initial magnetization of the ejecta, which in turn helps to constrain models for jet launching.

● **Probe the fundamental physics of particle shock-acceleration**. GRB 170817A was exceptional among GRBs for a number of reasons, including the remarkable stretch of a single power law of non-thermal emission observed from radio to X-rays [Troja *et al.* (2019)]. Whereas GRBs commonly show at least one spectral break within this range (either the synchrotron injection break due to the lower limit on energy of the shock-accelerated electron population often seen between radio and optical, or the synchrotron cooling break often observed between optical and X-rays), GRB 170817A allowed for an unprecedented accuracy in determining the electron energy power-law distribution slope, $p = 2.17$ (e.g. Troja *et al.* (2019)). It is noteworthy that except for its orientation relative to the observer, the afterglow modeling of GRB 170817A has not required extreme values for the other physical parameters that enter these models (explosion energy, circumburst medium structure, synchrotron efficiency parameters),

which suggests that observations of the same spectral regime across a wide range of frequencies are potentially the rule rather than the exception for counterpart observations, and additional tightly constrained measurements of p are to be expected.

This bodes well for the capability of MM counterparts observations to address a number of fundamental open questions in relativistic plasma physics of shock-acceleration.

• **Improve broadband afterglow calorimetry, and circumburst density measurements**. GRB afterglow jet models contain a range of physical parameters [Sari *et al.* (1998)]. Of these, energy and circumburst density set the time frame and flux level of the afterglow light curve. Jet geometry and orientation set the slopes of the light curve at different stages. Efficiency parameters for magnetic field generation and particle acceleration at the shock front set the flux level. All affect at which frequencies the transition points between the different power laws of the synchrotron spectrum can be found. With increasing sophistication in light curve modeling [van Eerten (2015)], observations no longer need to be simultaneous in order for them to be combined into constraints on these physical parameters, and late-time *Athena* observations will complement earlier broadband observations, while probing a unique dynamical regime of a blast wave seguing into trans-relativistic flow. Following the transition into a non-relativistic regime, the emission pattern of the jet attains isotropy, enabling a direct measurement of the jet energy (and potentially including observable counter-jet emission, although this is likely to be detectable in the X-rays only for strongly off-axis events at distances closer than 100 Mpc; see the late-time upturn of the light curves in Fig. 3). *Athena* thereby further broadens the potential of true MM modelling efforts (including e.g jet orientation constraints directly from GW observations in a comprehensive cross-messenger fit to data) to shed light on the physics of GRBs and on the nature of the engine.

3.1. *X-ray emission from kilonova*

The merger of a binary NS system can eject a large amount of material $M_{\rm ej} \gtrsim 0.01\,M_\odot$ at considerable velocity $\beta_{\rm ej} \gtrsim 0.1c$ [Hotokezaka *et al.* (2013)]. This material undergoes radioactive heating to produce a kilonova hours to days after the burst and then continues to expand homologously into the circumburst medium. In much the same way as the GRB afterglow, this material can sweep up ambient material and drive a synchrotron-producing forward shock wave: a kilonova afterglow [Nakar *et al.* (2011)].

Figure 3 (right panel) shows X-ray light curves of fiducial kilonova afterglows at a distance of 41 Mpc for various values of $M_{\rm ej}$ and $\beta_{\rm ej}$.

Direct observations of a kilonova afterglow can help characterize the kilonova material and identify details of its launching mechanism. The primary observables of an X-ray mission are the rising slope, the peak time, and the peak flux. The rising slope is a strong function of k and p. A clear measurement of the rising slope will constrain k, the degree of velocity stratification in the ejecta. The peak time depends on both $\beta_{\rm ej}$ and $M_{\rm ej}$ as well as the circumburst density n_0. If $\beta_{\rm ej}$ and $M_{\rm ej}$ are known to good confidence from prompt kilonova observations, then a measurement of the peak time will provide a measurement of n_0. On the other hand, if n_0 is known from the GRB afterglow, a measurement of the peak time will provide an independent constraint on $\beta_{\rm ej}$ and $M_{\rm ej}$. The peak flux is sensitive to the same parameters as the peak time, as well as the synchrotron parameters of its forward shock ϵ_e, ϵ_B, and ξ_N. This makes the absolute flux level a difficult observation to draw conclusions from, apart from bounding some combination of these parameters. The utility of kilonova afterglow observations will be greatest in a combined analysis with the prompt kilonova and the GRB afterglow.

The peak of the kilonova afterglow occurs $\sim 3 - 30$ years after the original burst, at a flux level that depends strongly on $\beta_{\rm ej}$ and $M_{\rm ej}$ as well as on the circumburst

environment density and energy fraction in non-thermal electrons and magnetic field [Ricci *et al.* (2021)]. The right panel of Figure 3 shows that, for fiducial values of these latter parameters, the kilonova afterglows of flows with $\beta_{\rm ej} \gtrsim 0.2$ should be detectable with *Athena*. These correspond to the afterglow of the "blue" kilonova observed in GW170817. The afterglows of slower ("red") kilonovae may be observable if they occur in denser environments.

3.2. *Observing strategy*

In line with the reasoning behind the *Athena* science requirements document, we propose to obtain *Athena* observations of a minimum of three sources in each bin in parameter space relevant for the case at hand. The gravitational wave sources of interest include NS-NS mergers and BH-NS mergers where the black hole mass/spin combination is such that the black hole will not swallow the neutron star whole, but instead disrupt it outside the innermost bound circular orbit, which is a necessary condition for the existence of an EM counterpart. The parameter space associated with these objects include; i) the inclination angle to the line of sight, ii) the spin of the newly formed NS or BH, iii) the initial black hole spin (for BH-NS mergers).

The *Athena* observing strategy will be based on GW observables that can be measured robustly from the gravitational-wave signal. While the spin of the final object (ii) might be the relevant parameter for understanding jet physics, it is not a quantity that can be determined directly from the gravitational waves with high accuracy. Fortunately, combining the masses of the binary components prior to merger and numerical simulations the spin can be determined. The masses of the two objects prior to merger can be measured directly from the gravitational-wave signal more robustly. For NS-NS mergers, the masses for the tens to hundreds of nearest events (and thus brightest events in X-rays) are expected to be measurable with percent precision with third-generation detectors [Grimm *et al.* (2020)]. As with BH-BH mergers, the largest errors are expected to arise from the uncertainties on the distance (which propagate to uncertainties on the source-frame masses; see, e.g., Vitale *et al.* (2017)). Measurement of the initial spin of the BH in a BH-NS system by third-generation detectors has not been studied in as great detail. The results, however, will likely be similar to those for BH-BH systems, where ten-percent accuracy on the spin for individual events is likely [Vitale *et al.* (2018)].

For the *Athena* observations we distinguish trigger observations which can be used to search for an X-ray EM counterpart and follow-up observations which will be obtained once the EM counterpart and a arcsecond localisation are known. For the latter observations, the nature of the EM counterpart, i.e., optical, near-infrared, radio and/or X-ray is not relevant in first instance.

4. *Athena* and LISA

LISA [Amaro-Seoane *et al.* (2017)] is the third large class mission of the ESA Cosmic Vision Program. It will explore the gravitational wave (GW) Universe in the 0.1 to 100 mHz frequency interval. Concurrent observations in GWs and X-rays by LISA and *Athena* can address a number of open questions in the domains of astrophysics, fundamental physics and cosmology:

• Accretion flows in violently changing spacetimes, formation of an X-ray corona and jet launching around newly formed horizons;

• Testing General Relativity as theory of gravity and measuring the speed of GWs and dispersion properties;

• Enhancement of the cosmic distance scale using GW sources as standard sirens.

The achievement of these synergistic science themes between LISA and *Athena* relies on a number of prospected GW sources. These are massive black hole coalescences in gas-rich environments; extreme and intermediate mass ratio inspirals (EMRIs/IMRIs) where a stellar black hole is skinning the horizon of a large black hole surrounded by an AGN disc; interacting double white dwarf systems present in large numbers in the Milky Way Galaxy.

4.1. *Synergy Science Topics*

Electromagnetic (EM) observations have revealed the occurrence of tight empirical relations between the black hole mass and quite a few host galaxy properties in the today universe [Kormendy *et al.* (2013)]. It is now widely accepted that during quasar/AGN activity, the launch of powerful winds by the black hole engine affected their accretion cycles and star formation jointly, self-regulating their growth in the host galaxy. One of the best explanations for these correlations invokes galaxy mergers conducive to massive black hole coalescences in gas-rich environments. These processes are central for establishing a key synergy between *Athena* and LISA.

LISA is expected to detect the GW signal from the coalescence of massive binary black holes in the largely unexplored interval between 10^4 and 10^7 $M_\odot$, forming in the aftermath of galaxy mergers, with a rate of a few to several tens per year [Barausse *et al.* (2020)]. LISA detections are likely to be dominated in number by lower mass systems at redshift $z > 5$, with low signal-to-noise ratio (S/N). However, up to several detections of black holes with masses $\geq 3 \times 10^5$ $M_\odot$ at $z < 2$ are expected per year. These events deliver the highest S/N in GWs, with a median error box small enough to be observable by *Athena* [Mangiagli *et al.* (2020)]. These are the most promising candidates of multi-messenger emission.

The detection of X-rays emitted by gas orbiting around coalescing massive black holes *contemporary* to the detection of the GW signal will let us correlate for the first time, the black hole masses and spins encoded in the GW waveform with the X-ray light and spectrum emitted by the surrounding gas. This will shed light on the behaviour of matter and light in the violently changing spacetime of a merger. Thus, the *additional science* resulting from joint observations will have a large impact on our knowledge of massive black holes as sources of both EM and GW radiation. The scientific return from concurrent observations can be summarized as follows:

The *pre-merger* phase, associated to the binary inspiral, might lead to an EM *precursor*. As the massive black holes spiral-in, X-ray emission is expected to be modulated in time, with characteristic variability correlating with the binary orbital motion or/and with relativistic fluid patterns rising in the non-axisymmetric circumbinary disc surrounding the two black holes [Tang *et al.* (2018); Khan *et al.* (2018); Bowen *et al.* (2018)] (cf. Fig. 4). This should be the distinguishing feature of a binary in the verge of merging. *Prompt, post-merger emission*, which is the most relevant for Athena, opens the door to the study of the mechanisms triggering accretion around a newly formed black hole. LISA observations provide the mass and spin of the black hole while X-ray observations measure the luminosity and spectra coming from disc re-brightening, corona emission, and launch of a jet from the spinning black hole. The X-ray window is particularly favorable as X-rays are known to come empirically from very close to the black hole horizon, i.e. a few Schwarzschild radii [Ricci *et al.* (2020)]. During the last phases of the inspiral gas can be tightly bound to each black hole in the form of two mini-discs. The system can thus be viewed as a superposition of two rapidly moving quasars almost all the way to the merger. X-ray Doppler modulations and relativistic beaming would characterize the emission.
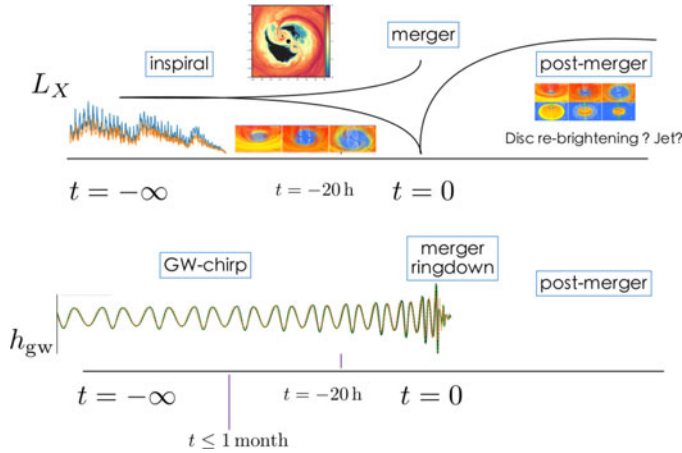
Figure 4. A cartoon depicting a possible trend of the X-ray luminosity during the inspiral (pre-merger), merger and post merger phase of two accreting massive black holes in a binary system. The insets in the upper panel are: from Bowen *et al.* (2018) (top) illustrating the relativistic flow pattern around two non-spinning black holes close to merging; from Tang *et al.* (2018) showing the model X-ray light curve; from Khan *et al.* (2018) showing the circumbinary disc and the incipient jets that naturally form both prior to and after the coalescence. The bottom panel shows the GW amplitude as a function of time. The GW emission dies out when the ringdown phase has ended.

Table 2. Observational-based predicted number of expected SMBH merging events visible by *Athena* and LISA over 5 years.

	$M=10^6 \ M_\odot$	$M=10^7 \ M_\odot$
$z = 1$	1.5	0.5
$z = 2$	12	1.2

4.2. *Localization and sample selection*

For a significant fraction of binaries with $M \approx 3 \times 10^5 - 10^7 \ M_\odot$ up to $z \sim 2$ LISA delivers a location error that can be observed in the post-merger phase with the *Athena*/WFI. We define a *Golden Binary* as being composed of objects such that the error box derived *after* the merger is smaller than the WFI FoV (0.4 deg^2).

For the highest S/N events the localization derived in the inspiral phase can allow *Athena* to repoint *before* the merging takes place. We define a *Platinum Binary* as being composed of objects whose localisation error, determined 5 hours before the merger, is smaller than the WFI FoV. The timing is consistent with the *Athena* capability of carrying out a ToO in 4 hours. The *Platinum Binary* comprises a fraction of binary mergers with mass within $3 - 10 \times 10^5 \ M_\odot$ below $z \approx 0.5 - 1$, and thus likely to be rare (Tab. 2). However, for the *Platinum Binaries* the inspiral and merging phases can both be observed with *Athena*, opening the intriguing perspective to observe in X-rays the BH merging event in the act. With a proper observing strategy, *Athena* can actually start observing a few days before the final binary coalescence. At this time the localisation error of objects in the *platinum binary* is ≈ 10 deg^2, an area that can be effectively covered by tiling WFI observations in about 3 days.

An error box of 10 deg^2 can be covered with the *Athena*/WFI in 3 days with a raster scan of at least 23 observations of $\simeq 9$ ks each. Once the LISA event localization is comparable to, or smaller than the *Athena*/WFI FoV, *Athena* could stare to the predicted error box up to the time of the merger. With the improvement of the LISA localization

Table 3. Fluxes (0.5-2 keV) in erg cm^{-2} s^{-1} and exposure times (in brackets) to detect a X-ray unobscured AGN at the Eddington limit with the current configuration of the *Athena* mirror+WFI.

	M=10^5 M$_\odot$	M=10^6 M$_\odot$	M=10^7 M$_\odot$
$z = 1$	5.3×10^{-17} (250 ks)	5.3×10^{-16} (7 ks)	5.3×10^{-15} (<1 ks)
$z = 2$	1.1×10^{-17} ($\gtrsim$1 Ms)	1.1×10^{-16} (70 ks)	1.1×10^{-15} (3 ks)

the *Athena* pointing strategy can be optimized to cover the most likely location of the trigger at any time.

How likely is it that the X-ray glow is sufficiently bright to be detectable by the WFI? The answer is in Tab. 3, where we show the expected fluxes and required *Athena* exposure time to detect an AGN at the Eddington limit, assuming an X-ray to bolometric luminosity ratio of 30, and the sensitivity of the WFI averaged over its full FoV. These results indicate that follow-up of Black Holes (BH) of mass 10^6 M$_\odot$ could require considerable *Athena* observing time, particularly if the source is obscured. These results show that an unobscured AGN associated with a merger of SMBHs of masses $\sim 10^6 - 10^7$ M$_\odot$ at $z > 1$ can be detected anywhere within the *Athena* FoV in $\sim$ a few ks, increasing to $\sim$70 ks for lower mass super massive black hole mergers (SMBHMs) at $z = 2$. If the associated AGN is obscured (and thus is most efficiently detected at 2-10 keV energies) then the exposure times increase, requiring day-long exposures except for the most massive, and therefore potentially X-ray brightest, SMBH pairs. Lower mass, SMBHMs at $z > 2$ that are associated to obscured AGN are likely to remain undetectable, even in extremely deep exposures, due to the impact of source confusion. These numbers provide the rationale for searching for the X-ray counterpart of a SMBHM event even prior to the merging occurs.

5. *Athena*, neutrino and VHE gamma-ray observatories: ICECUBE, KM3NET & CTA

Many X-ray sources have non-thermal radiation components over a wide range of the electromagnetic spectrum. In some cases their spectral energy distribution is even dominated by non-thermal radiation. Examples are active galactic nuclei (AGN) in all forms, gamma-ray bursts (GRBs), supernova remnants (SNRs), and pulsar wind nebulae (PWNe). These non-thermal emission components are invariably the results of particle acceleration by collisionless shocks, or through magnetic reconnection processes. In the radio and X-ray bands the non-thermal emission is most likely synchrotron radiation, caused by relativistic electron and/or positron populations. X-ray emission in particular is important for detecting the highest energy electrons/positrons (typically > 10 TeV for magnetic fields below 1 mG). These electron/positron populations, collectively referred to as leptons, also cause inverse Compton scattering and non-thermal bremsstrahlung in gamma rays.

However, the acceleration processes themselves are often not confined to leptons; in fact in many cases the dominant population of accelerated particles consists likely of atomic nuclei, i.e. hadrons. The relativistic hadronic populations may be energetically more important, but their presence can only be inferred from gamma-ray observations and/or neutrino detection. The latter is a unique signature of accelerated hadrons, whereas gamma rays can either be hadronic, or (as stated above) leptonic in origin.

The accelerated particles will eventually escape their acceleration sites, thereby filling the Galaxy and even intergalactic space with high energy hadrons. We know of these hadrons as we observe them on Earth as CRs; yet, deflections in turbulent magnetic fields before arrival do not permit to directly trace their origin. Less than 1% of the CRs are leptonic, so in order to understand the origin of >99% of CRs we need

gamma-ray and very-high-energy (VHE) neutrino observations. Revealing the presence of CRs, and thereby pinpointing the astrophysical sources of CRs, are the main science drivers for present and future gamma-ray observatories, and high-energy ($\gtrsim TeV$) neutrino detectors.

Since the acceleration mechanisms for hadrons and leptons are the same, X-ray observations are important to probe the active acceleration conditions, since the X-ray synchrotron emitting electrons lose their energy on short time scales. Moreover, X-ray observations provide superior angular resolution and statistics, and the thermal X-ray component, if present, helps to understand the conditions in which particles are accelerated, as well as provide a probe of the local plasma and radiation energy densities, with which accelerated particles interact.

This in a nutshell shows the synergy between *Athena* on the one hand, and the CTA gamma-ray observatory, and the HE neutrino detectors IceCube and KM3Net on the other hand: *X-ray observations* give a handle on the *accelerated leptons* and the properties of the local environment of CR sources, and *gamma-rays and HE neutrinos* detections are able to reveal the presence and spectrum of (ultra)relativistic *hadrons*. The X-ray observations are then essential to translate the gamma-ray and neutrino measurements into the CR energy budget of these CR sources.

By the time *Athena* is launched we expect that CTA-North and South will be the most sensitive VHE gamma-ray observatories, and that the most sensitive HE neutrino detectors will be IceCube, perhaps in an upgraded form, and KM3NeT. The combination of *Athena* X-ray observations with neutrino and gamma-ray detections will lead to better disentanglement of non-thermal leptonic and hadronic populations. Moreover, the much better spatial resolution in X-rays and event statistics will help to accurately pinpoint the acceleration sites, as well as characterise the overall environment in sources of CRs.

5.1. *Synergy Science Themes*

One of the main scientific drivers for CTA, IceCube, and KM3NeT is the question: "what is the origin of cosmic rays?" Cosmic rays were discovered by Victor Hess in 1911, and since the 1930s it was realised that the mysterious "rays" were in fact highly-energy charged particles ($> 10^8$ eV) entering the Earth's atmosphere. The cosmic-ray (CR) spectrum has roughly a power-law distribution with index -2.7 from 10^9 eV up to $\sim 10^{19}$ eV, but a spectral softening around 3×10^{15} eV (CR "knee"), and a subsequent hardening around 5×10^{18} eV (CR "ankle") which is usually explained by the idea that sources in the Milky Way are responsible for accelerating protons up to the knee, whereas particles in excess of the ankle must be of extragalactic origin. The range between the knee and the ankle is a transition between the two components. Apart from the question of what the sources of Galactic and extragalactic CRs are, a related question is how these sources are capable of accelerating particles to very high energies, and what fraction of the energy budget goes to the acceleration of particles.

For the energy budget it is also important to distinguish the leptonic and hadronic components. Leptons are radiatively efficient, and produce synchrotron radiation from radio (~ 10 MHz) to X-ray frequencies ($\sim 10^{19}$ Hz), but the latter only if lepton acceleration is very fast. The same electrons/positrons may also Compton up-scatter background photons, causing non-thermal X-ray to gamma-ray emission. However, the CRs on Earth consist of less than 1% of leptons. It is, therefore, likely that the non-thermal populations in sources of CRs consist primarily of hadronic CRs. These hadronic CRs do not produce a direct tracer of their existence in traditional astrophysical wavelength bands like radio, optical or X-rays, but instead produce gamma rays and neutrinos.
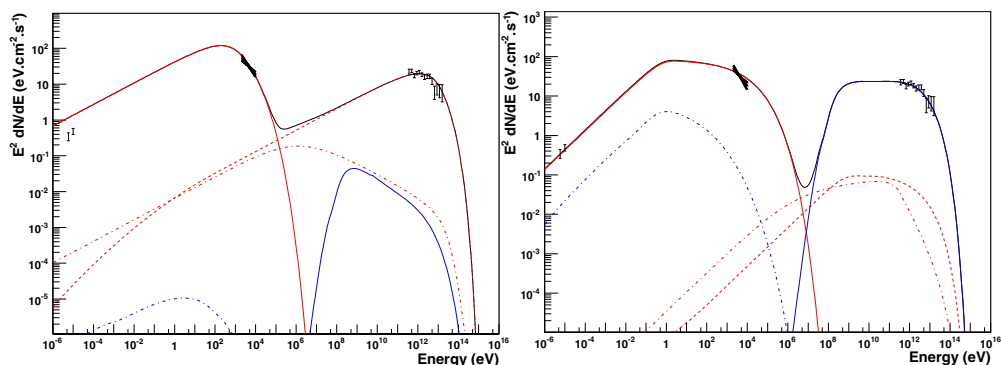
Figure 5. Example of a broad spectral energy distribution displaying the non-thermal radiative out from the SNR RX J0852.0-4622, taken from Aharonian *et al.* (2007). In both panels the emission below 1 MeV is synchrotron radiation, whose brightness depends on the population of electrons/positrons and magnetic-field strength. The component above 1 MeV (red) is dominated by inverse Compton scattering (red dashed line) from local radiation fields in the left-hand panel and pion decay (blue) in the right-hand panel. Inverse Compton scattering depends on local radiation fields such as cosmic-microwave background, stellar light, or — in the case of GRBs and AGN — synchrotron emission from the source itself. In the case of blazars and GRBs, relativistic effects should be taken into account. Pion production depends on the local gas density. In the case of SNR shells these can be determined from thermal X-ray emission. For blazars it is theorized that there is a pion production from proton-photon collisions. Identifying such a component would prove that —apart from electrons— also protons are accelerated.

Fig. 5 shows the non-thermal spectral-energy distribution of a young supernova remnant, with the characteristic two peaked structure, one in X-rays and one in TeV gamma rays. In this case it is not clear whether the gamma-ray peak is caused by leptonic or hadronic radiation processes.

The detection of high energy neutrinos can be directly linked to CR hadrons. For gamma-ray emission it is not immediately clear whether the emission is caused by hadronic or leptonic CRs, as leptons also produce gamma-ray emission through inverse Compton scattering, and (less likely) non-thermal bremsstrahlung.

Identifying X-ray synchrotron emission can help to disentangle hadronic from leptonic gamma-ray emission, because X-ray synchrotron emission is caused by roughly the same energetic leptons ($\gtrsim 10$ TeV) as VHE inverse Compton emission. The X-ray synchrotron brightness depends on the number density of leptons and strength of the local magnetic field, whereas the gamma-ray emission also depends on the number density of leptons, but also on the radiation energy density. The latter can often be estimated, so that there is only one free parameter left to be determined: the strength of the magnetic field. Under the assumption of purely leptonic emission (and a single-emitting zone scenario) one can estimate the magnetic field. If this magnetic field estimate is unphysically low, one can conclude that the gamma-ray emission is likely not leptonic in nature, and an additional hadronic component is necessary. However, what are plausible magnetic field strengths is open to debate. So the ultimate proof for the presence of contribution by hadronic processes to the gamma-ray spectrum of an astrophysical source is to detect high-energy neutrinos from this source.

The high relevance of X-ray observations to resolve this puzzle can be seen by the following argument [Murase *et al.* (2016)]. Strong X-ray emission by the region that is also responsible for CR acceleration allows for efficient neutrino production via CR/photon ($p\gamma$) interactions. The energy of secondary neutrinos from pion decay can be estimated by the center-of-mass energy of the Δ-resonance in the shock environment, assumed to move

at a bulk Lorentz factor Γ. The secondary neutrino energy E_ν and target photon energy ε_t observed in the observer's frame are then related as $\varepsilon_t \simeq 6 \text{ keV}(\Gamma/10)^2/(E_\nu/100 \text{ TeV})$. In other words: strong X-ray sources are excellent candidate sources for the neutrino emission observed in IceCube. At the same time, the strong X-ray background would allow to absorb gamma rays produced in hadronic emission ($\gamma\gamma \to e^+e^-$ interactions), making these sources less prominent in GeV–TeV gamma-ray observatories [Murase *et al.* (2016)]. The minor contribution to the diffuse neutrino emission observed by IceCube by gamma-ray blazars [Aartsen *et al.* (2017)] is another motivation for gamma-opaque AGN as neutrino sources.

Another example pertains the conversion of gamma-ray and neutrino flux to CR energy in SNR. X-ray measurements, as obtained by Athena, are crucial: accurate modeling of the thermal emission will provide the density and composition of the SNR as a function of location, important for the hadronic interaction model, needed for converting gamma-ray fluxes into total hadronic CR energies. Thermal X-ray emission can also inform us by other means about the CR acceleration properties of SNRs, which will provide information that complements gamma-ray and neutrino signals. In this case one has to use Athena/X-IFU's ability to measure line broadening. In SNRs line broadening can be either due to line of sight bulk motion, or due to thermal Doppler broadening. Thermal Doppler broadening provides a way to measure the ion temperature. Traditional CCD spectra can only measure electron temperatures. Only with high-resolution spectroscopy and imaging can the ion temperature be measured and only Athena can do that sufficiently close to the edge of the remnant. The Athena/X-IFU provides the spatial resolution to isolate regions close to the SNR edge, as well as a spectral resolution sufficient to measure line broadening of a few hundreds of km/s and separate thermal line broadening from bulk motions. The link with CR acceleration is that the ion temperature is expected to be lower if CR acceleration is more efficient. By accurately measuring ion temperatures we can measure or set stringent limits on the CR acceleration efficiency of shocks [Vink *et al.* (2010)].

5.2. *Observational strategy*

The Athena/WFI and Athena/X-IFU will be able to provide identification and characterization of the GeV to TeV gamma-ray sources, the majority of which should be bright in X-rays, in order to constrain the nature of diffuse VHE emission and localize particle acceleration. On another hand, a dedicated extragalactic survey will cover one fourth of the sky and will be enable to probe new source populations such as extreme blazars (whose inverse Compton peak is located above 100 GeV) as well as investigate further the content of relativistic jets and the galaxy cluster formation shocks. Understanding further these sources will require multi-messenger observing campaigns including both *Athena* and neutrino telescopes. While these science cases do not require very fast response from Athena, they will certainly require extended observations by *Athena* to characterize the spectrum and, for diffuse sources, their spatial and spectral properties, along with multi-instrument observing campaigns that need to be planned and coordinated well in advance.

Next generation neutrino observatories will deliver typical angular resolution for high-energy neutrinos within the WFI FoV, that should be sufficient to trigger *Athena* follow-up as ToO observations. If the candidate is a catalogued source, *Athena* follow-up observations can use the X-IFU. Otherwise, a refined position of the source might be obtained first through observations with large FoV X-ray instruments. In the same energy range, if the source is sufficiently bright, its transient behaviour might also be confirmed by large survey archival data such as the eROSITA survey.

6. Conclusions

Astronomy has evolved in time from an ensemble of wavelength-specific sectors into a multi-wavelength enterprise, and is now taking a step further into the multi-messenger era. In this paper we have highlighted some of the many synergies between *Athena* and some of the key multi-messenger facilities that should be operative concurrently with Athena [Piro *et al.* (2021)].

References

Aartsen, M. G. *et al.* 2017, *ApJ*, 45
Abbott, R. and Abbott, T. D. and Abraham, S. *et al.* 2021, *Physical Review X*, 11, 021053
Ade, P.A.R. *et al.* 2016, *A&A*, 594, A13
Aharonian, F., Akhperjanian, A. G., Bazer-Bachi, A. R. *et al.* 2007, *ApJ*, 661, 236-249
Amaro-Seoane, P., Audley, H., Babak, S. *et al.* 2017, *arXiv e-prints*, 1702.00786
Barausse, E., Dvorkin, I., Tremmel, M. *et al.* 2020, *ApJ*, 904, 16
Barret, D. *et al.* 2021, in preparation
Bowen, D. B., Mewes, V., Campanelli, M. *et al.* 2018, *ApJl*, 853, L17
Ghirlanda, G., Salafia, O. S., Paragi, Z. *et al.* 2019, *Science*, 363, 968-971
Grimm, S. and Harms, J. 2020, *Phys. Rev. D*, 102, 022007
Hall, E. 2019a, *LIGO Document T1800084-v6*
Hall, E., Evans, M. 2019b, *Classical and Quantum Gravity*, 36, 225002
Hall, E. and Vitale, S. 2019c, *LIGO Document G1900803-v1*,
Hotokezaka, K., Kiuchi, K., Kyutoku, K. *et al.* 2013, *prd*, 87,024001
Khan, A., Paschalidis, V., Ruiz, M. *et al.* 2018, *PRD*, 97, 044036
Kormendy, J. and Ho, L. C. 2013, *ARAA*, 51, 511-653
Lamb, G. P., Lyman, J. D., Levan, A. J. *et al.* 2019, *ApJl*, 870, L15
Mangiagli, A. and Klein, A. and Bonetti, M. *et al.* 2020, *PRD*, 102, 084056
Meidinger, N. and Albrecht, S. and Beitler, C *et al.* 2020, *Society of Photo-Optical Instrumentation Engineers (SPIE) Conference Series*, 11444, 114440T
Mooley, K.P., Frail, D.A., Dobie, D. *et al.* 2018, *ApJl*, 868, L11
Mooley, K. P., Deller, A. T., Gottlieb, O. *et al.* 2018, *Nature*, 561, 355-359
Murase, K., Guetta, D., Ahlers, M. 2016, *PhysRevLett.*, 116,
Nakar, E. and Piran, T. 2011, *Nature*, 478, 82-84
Nousek, J. A. *et al.* 2006, *ApJ*, 642, 389-400
Piro, L., Ahlers, M., Coleiro, A. *et al.* 2021, *arXiv:2110.15677*
Ricci, C., Kara, E., Loewenstein, M. *et al.* 2020, *ApJl*, 898, L1
Ricci, R., Troja, E., Bruni, G. *et al.* 2021, *MNRAS*, 500, 1708-1720
Sari, R., Piran, T., Narayan, R. *et al.* 1998, *ApJl*, 497, L17-L20
Sathyaprakash, B., Bailes, M., Kasliwal, M. M., *et al.* 2019, *BAAS*, 51, 276
Tang, Y., Haiman, Z., MacFadyen, A. 2018, *MNRAS*, 476, 2249-2257
Troja, E., Piro, L., Ryan, G. *et al.* 2018, *MNRAS*, 478, L18-L23
Troja, E., van Eerten, H., Ryan, G. *et al.* 2019, *MNRAS*, 489, 1919-1926
Troja, E., van Eerten, H., Zhang, B. *et al.* 2020, *MNRAS*, 498, 5643-5651
van Eerten, H. J. 2015, *Journal of High Energy Astrophysics*, 7, 23-34
Vink, J., Yamazaki, R., Helder, E. A., et al. 2010, *ApJ*, 722, 1727
Vitale, S. and Evans, M. *et al.* 2017, *Phys. Rev. D*, 95, 064052
Vitale, S. and Whittle, C. 2018, *Phys. Rev. D*, 98, 024029
Vitale, S., Farr, W. M., Ng, K., Rodriguez, C. L. 2019, *ApJ*, 886, L1
Zhang, B., Fan, Y. Z., Dyks, J. *et al.* 2006, *ApJ*, 642, 354-370